EPR and ENDOR Study of Radiation-Induced Radical Formation in Purines: Sodium Inosine Crystals X-irradiated at 10 K

Sibel Tokdemir and William H. Nelson*

Department of Physics and Astronomy, Georgia State University, P.O. Box 4106, Atlanta, Georgia 30302-4106

Received: January 11, 2006; In Final Form: March 20, 2006

X-irradiated single crystals of sodium inosine (Na^+·Inosine$^-$·2.5H_2O), in which the hypoxanthine base is present as the N1-deprotonated anion, were investigated using K-band (24 GHz) electron paramagnetic resonance (EPR), electron−nuclear double resonance (ENDOR), and ENDOR induced EPR (EIE) techniques at 10 K. At least five different radicals were present immediately after irradiation at 10 K. **R1**, which decayed upon warming the crystals to 50 K, was identified as the electron-loss product of the parent N1-deprotonated hypoxanthine base. Hyperfine couplings to HC8 and HC2 were fully characterized with ENDOR spectroscopy, and the identification was supported by DFT calculations. **R2**, which also decayed on warming to 50 K, exhibited nearly equal couplings to HC2 and HC8. Taken in combination with an extensive set of DFT calculations, the experimental results indicate that **R2** is the (doubly negative) product of electron-gain by the initially anionic N1-deprotonated hypoxanthine parent. **R3**, which exhibited hyperfine coupling only to HC8 could not be identified. **R4**, which persisted on annealing to 260 K, exhibited one large α-proton hyperfine coupling which was fully characterized by ENDOR. Based on DFT calculations and the experimental data, **R4** was identified as the product of net H-abstraction from C5′. The remaining HC5′ was the source of the measured α-proton coupling. **R5**, present at low temperature and the only observable radical after warming the crystals to room temperature, was identified as the C8−H addition radical. The α-coupling to HC2 and *β*-couplings to the pair of C8 methlyene protons were fully characterized by ENDOR.

Introduction

This work continues a series of investigations into the ionization-initiated radical products of hypoxanthine derivatives. The overall goal of the investigations is to understand and develop descriptions of radiation-initiated radical mechanisms important for DNA ionization. Although it is not a natural component of DNA, hypoxanthine is a useful subject because of its similarities to, and differences from, the natural purine components of DNA, adenine and guanine. In particular, one mechanism potentially decisive for the stability or transience of a radical species is its capability to rapidly donate or accept protons as a charge neutralization mechanism following electron loss or gain.[1,2] As is shown by the structures below, specific differences among hypoxanthine, guanine, and adenine are the distribution of polar regions at positions 1, 2, and 6. These regions serve as proton acceptors or donors with other polar species in their immediate molecular environment and thereby are centrally important to whether proton transfers can occur rapidly following one-electron ionization of the purine.

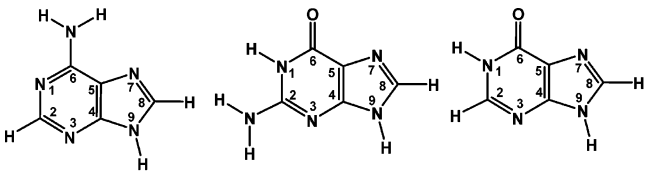

Adenine *Guanine* *Hypoxanthine (Hx)*

The initial study of this series focused on inosine, the riboside of hypoxanthine.[3] More recently, we reported results from hypoxanthine crystallized from acidic solutions causing protonation at N7.[4,5] This report focuses on inosine crystallized from basic solutions causing deprotonation at N1 (see the structure below). This N1-deprotonated anionic form of the hypoxanthine base has no remaining N−H protons; as a result, the base itself has no capability to deprotonate on electron loss. Thus, this set of molecules offers the following variety of protons attached to nitrogen positions in hypoxanthine: protons at N1 and N7 (N7-protonated hypoxanthine), proton at N1 (inosine), and none (N1-deprotonated hypoxanthine).

Study of the N7-protonated hypoxanthine crystals clearly identified two major products of ionization-induced proton transfer involving the purine: deprotonation at N7 following electron loss, and protonation at N3 following electron gain. Unfortunately, in the inosine study, it was not possible to conclusively identify the radical products of hypoxanthine, although possibilities included electron loss with no deprotonation and/or with deprotonation at N1. Thus, the specific goal for this study was to clarify the results from inosine, while the broader goal was to characterize the response to oxidation of a purine system with no readily available avenue for charge neutralization by deprotonation.

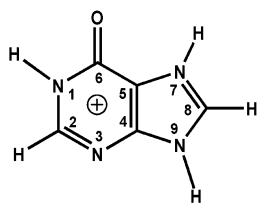

N7-protonated hypoxanthine

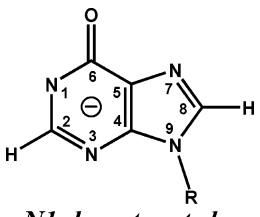

N1-deprotonated Hypoxanthine

* Corresponding author. Telephone: 404-651-1970. Fax: 404-651-1427. E-mail: wnelson@gsu.edu.

10.1021/jp0602169 CCC: $33.50
Published on Web 05/04/2006

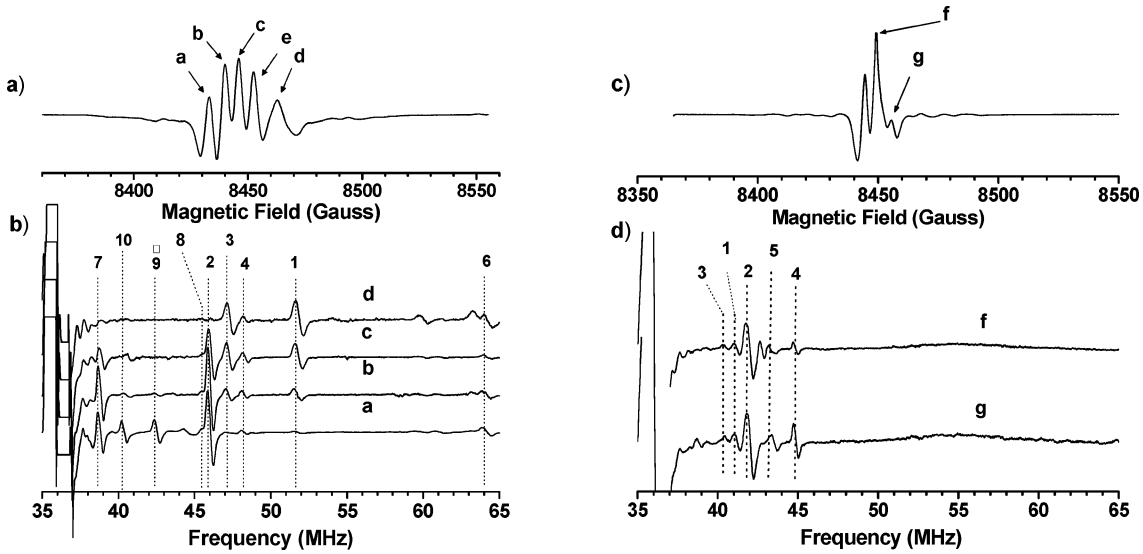

Figure 1. (a) EPR (second derivative) and (b) ENDOR spectra of $Na^+ \cdot Inosine^- \cdot 2.5H_2O$ recorded at 10 K with the external field parallel to the $\langle b \rangle$ axis. Magnetic field positions labeled a−d in part a indicate the settings for the ENDOR spectra shown in part b. Field setting e was used for the ENDOR shown in Figure 3. (c) EPR and (d) ENDOR spectra recorded at 10 K with the external field parallel to the $\langle c \rangle$ axis. Magnetic field positions f and g in part c indicate the settings for the ENDOR spectra in part d.

Experimental Section

High-quality crystals of $Na^+ \cdot Inosine^- \cdot 2.5H_2O$ were prepared from commercial inosine (Sigma I4125, used as received) by slow evaporation from high-pH aqueous solutions at room temperature. Typical solutions consisted of 0.2 M inosine in 0.3 N NaOH. Crystals formed from open solutions within 3−4 days and solutions kept in a desiccator gave crystals after 1 day. Deuterated crystals also were grown in a corresponding manner from NaOD and D_2O solutions kept in a desiccator. (It turned out that none of the couplings detected by ENDOR were from exchangeable protons.) Under these conditions, the sodium salt crystallized with the inosine molecule in the anionic form via deprotonation at N1 as is mentioned above. The molecule with the standard numbering system is shown below:

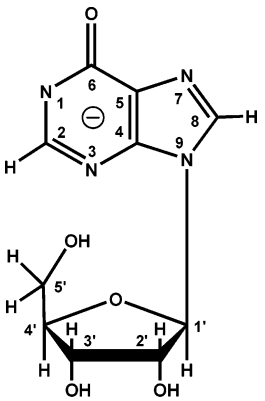

N1-deprotonated inosine structure

The crystallographic and molecular structure of $Na^+ \cdot Inosine^-$ was reported by Klüfers and Mayer who found the crystals to have orthorhombic symmetry belonging to space group $P2_12_12$.[6] Because of the orthorhombic symmetry, the experimental results given below are expressed in an *xyz* system based on the *abc* crystallographic axes. Moreover, the good quality of the crystals permitted analysis and reporting of the hydrogen atom positions.

Following irradiation of the crystals to ca. 100 kGy, data were collected from three independent planes of rotation: about the $\langle a \rangle$, $\langle b \rangle$, and $\langle c \rangle$ axes. To resolve the Schonland ambiguity,[7] data was collected from a check plane by rotation of a crystal about an axis with the polar coordinates $\theta = 163°$ and $\phi = 136°$. Data from each plane was collected from a fresh crystal and the consistency of the measurements indicates the repeatability of the data. Previous reports describe the experimental procedures of X irradiation followed by K-band (ca. 23.7 GHz) EPR, ENDOR, and ENDOR−Induced EPR (EIE) measurements at liquid helium temperatures. We note that the EPR spectra are presented in second derivative format, that the ENDOR is in first derivative format, and that the free-proton frequency for ENDOR at K-band is approximately 36.0 MHz. Details of the data collection and analysis methods were previously described.[5,8]

To aid in identifying the radical products, hyperfine couplings from feasible structures following geometry optimizations were calculated using Gaussian 03 for Windows (G03W).[9] All computations used DFT methods with the B3LYP functional,[10] optimizations used the 6-31G basis set, and hyperfine couplings were computed with the 6-311G basis.[11] More detail on the computational procedures is given in the discussions of the specific results below. Previous reports have shown that this general approach predicts hyperfine couplings which correlate well with experimental results.[12]

As well, characteristic directions associated with the anisotropic couplings from EPR crystallography are very helpful in identifying the radical structures. Recent work has shown that structures computed from crystallographic coordinates using the NOSYMM option provide dipolar coupling eigenvectors which correlate well with the experimental results.[13,14] Evidently with this computational approach, molecular reorientations on radical formation are described well by the geometry changes during optimization. Thus, for the analyses described below, the G03W data sets were prepared with Cartesian coordinates obtained from the crystallographic data and the NOSYMM option.

Results and Discussion

Figures 1 and 2 show EPR, ENDOR, and EIE spectra recorded at 10 K following irradiation at that temperature. Numbers labeled on the ENDOR lines correspond to the proton couplings. EIE and warming techniques were used for grouping

TABLE 1: Hyperfine Couplings for R1[a] Formed in Na^+·Inosine$^-$·2.5H_2O X-Irradiated at 10 K

coupling (line)	isotropic value[b,c]	principal value[b,c]	eigenvectors[b] ⟨a⟩	⟨b⟩	⟨c⟩
$R1_1$ (line 2)	−16.38 (2)	−24.83 (2)	0.304 (2)	−0.767 (1)	−0.565 (1)
		−17.68 (2)	−0.853 (1)	−0.483 (2)	0.198 (1)
		−6.62 (2)	0.424 (1)	−0.422 (1)	0.801 (1)
$R1_2$ (line 7)	−3.56 (5)	−6.40 (3)	0.482 (19)	−0.816 (12)	−0.318 (6)
		−5.43 (3)	−0.846 (12)	−0.528 (19)	0.071 (6)
		1.15 (9)	0.226 (5)	−0.235 (7)	0.945 (2)
N1[d]	3.43	4.98	normal to the ring		
		2.66	in the plane of the ring		
		2.66	in the plane of the ring		
N3[d]	12.93	30.66	normal to the ring		
		4.06	in the plane of the ring		
		4.06	in the plane of the ring		

directions from crystal structure	eigenvectors[b] ⟨a⟩	⟨b⟩	⟨c⟩
base perpendicular	−0.86845	−0.45239	0.20283
C8−H bond direction	0.36318	−0.30203	0.88141
C2−H bond direction	0.12216	0.15018	0.98108

[a] Structure **1**. [b] Numbers in parentheses are the estimated uncertainties in the respective values as reported by the statistical analysis. [c] Couplings in MHz. [d] See Spectrum Simulation for a description of the method used to evaluate these.

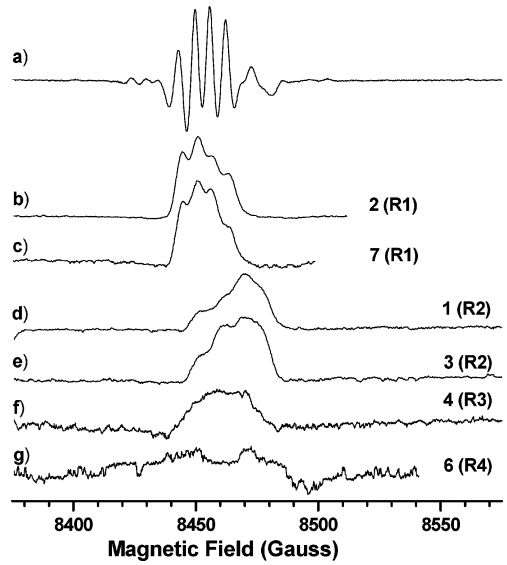

Figure 2. (a) EPR (second derivative) and (b−g) EIE responses from each ENDOR line indicated in Figure 1b. The EIE patterns are similar for lines 2 and 7 which were assigned to **R1**. Likewise, EIE from lines 1 and 3 are similar and they were assigned to **R2**. **R3** has only one coupling indicated by line 4; **R4** also has only one detectable coupling indicated by line 6.

the radicals. As is explained below, the data indicates the formation and stabilization of at least five different radicals: **R1**, **R2**, **R3**, **R4**, and the C8 H-addition radical.

Radical R1: The Electron-Loss Radical. On the basis of the similar EIE patterns of lines 2 and 7, shown in Figure 2, these two lines were assigned to the same radical. Analysis of their full angular dependence, (shown in Figure S1 of the Supporting Information) gave the results listed in Table 1. (All nitrogen couplings listed in Table 1 were obtained with the EPR spectrum-simulation methods discussed below.) As is shown in Figure 3, lines 2 and 7 disappeared on annealing the crystals to 50 K.

Coupling 2 is characteristic of an α-coupling to HC8 since the eigenvectors for minimum and intermediate values deviate 9.0 and 2.0° from the crystallographic C8−H bond direction and the base perpendicular, respectively. The isotropic component of coupling 2 indicates C8 spin density of 0.23 ($Q^{\alpha}_{iso} = -70$ MHz[15]) while the dipolar component indicates $\rho(C8) = 0.25$ ($Q^{\alpha}_{dip} = 38.7$ MHz[15,16]). Although coupling 7 is assigned to HC2, it has more unusual properties. Specifically, the two negative components listed in Table 1 (**R1**$_2$) are nearly equal and noticeably larger in magnitude than the positive component; these are properties more characteristic of a point dipole interaction (β-like) than a standard α-coupling.

Previous EPR/ENDOR study of the neutral inosine molecule in anhydrous inosine crystals found a radical—named RI in that study—with a pair of proton couplings very similar to those from lines 2 and 7 in this study.[3] On the basis of the similarities of the coupling tensors and parent molecules, it seems certain that **R1** of this study and RI of the earlier one are from a radical with the same structure.

To aid in the identification of **R1**, we calculated couplings expected from several radical structures based on electron loss (oxidation) by the parent. Of these, Hx^0_{-1} and $Hx^{-1}_{-1,-9}$ (shown as structures 1 and 2, respectively)[17] gave couplings similar to

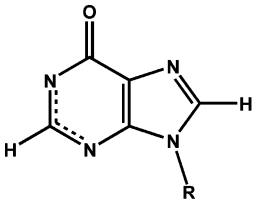

Structure 1: Hx^0_{-1}

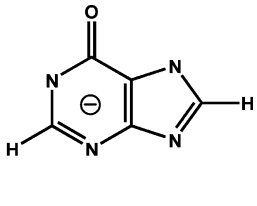

Structure 2: $Hx^{-1}_{-1,-9}$

those associated with lines 2 and 7 (see Table 2). For $Hx_{-1}{}^0$, the calculated HC8 coupling (eigenvalues and eigenvectors) are virtually identical to those obtained experimentally for line 2. In addition, this structure is readily identifiable as the product of electron loss in Na^+:Ino$^-$, and that of electron loss followed by deprotonation at N1 of inosine.

Also for Hx^0_{-1}, the coupling values predicted for HC2 match those of line 7 very well. However, the calculated eigenvectors correspond poorly to the experimental results for line 7. Specifically, the calculated $\hat{V}_{mid}$ corresponds to the experimental $\hat{V}_{max}$ and vice versa. Close inspection of the computational results shows predicted spins at N1, C2, and N3 of 0.13, −0.05,

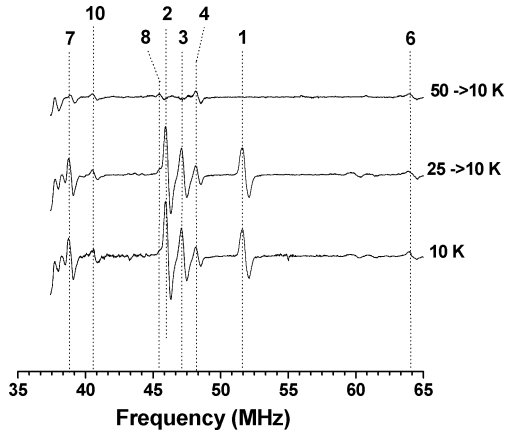

Figure 3. ENDOR warming study for $Na^+ \cdot Inosine^- \cdot 2.5H_2O$. The magnetic field was parallel to the $\langle b \rangle$ axis and the field was set to the peak labeled e in Figure 1a. ENDOR lines 2, 7, 1, and 3 all disappeared on warming to 50 K. Only lines 4, 6, 8, and 10 persisted at higher temperatures.

and 0.28, respectively, creating an allyl-like arrangement. The small amount of spin at C2 means that the coupling to HC2 arises from the composite of all three centers of spin: an α-interaction from the small negative spin on C2, and the dipolar component of β-interactions from the positive spin on N1 and N3. We note that the experimentally estimated coupling to N3 is a close match to that predicted, but the experimental value for N1 is much less than predicted.

Because the HC2 coupling predicted for the $Hx^{-1}_{-1,-9}$ structure also is a good match for the experimental result from line 7, it is necessary to consider this as a possibility for **R1**. Formation of $Hx^{-1}_{-1,-9}$ from Na^+:Ino^- would be the net result of electron loss and cleavage of the N9−C1′ bond. Normally, cleavage of CN bonds is considered an unlikely mechanism for ionization-initiated products in solids. However, the recent discovery that low-energy electrons (LEE) lead to DNA strand breakage[18] indicates the need to consider the LEE mechanism in the analysis of direct ionization effects. Taken in combination with the experimental values, the computational results provide no conclusive basis for distinguishing between Hx^0_{-1} and $Hx^{-1}_{-1,-9}$ as the identity of **R1**. Computational results from both structures reproduce the experimental HC8 coupling well;, However, the calculations for the HC2 coupling from $Hx^{-1}_{-1,-9}$ agree better with experiment while those from Hx^0_{-1} more nearly match experimental estimates for the N3 nitrogen couplings. It is easy to understand how Hx^0_{-1} could occur in both Na^+:Ino^- and inosine since it is product of simple electron loss in the former, and of electron loss followed by deprotonation at N1 in the latter. In contrast, for $Hx^{-1}_{-1,-9}$ to be a product of inosine, it is necessary that the parent undergoes two bond cleavages (i.e., N1−HN1 and N9−C1′), and it is difficult to envision both events occurring. Thus, we propose the structure Hx^0_{-1} as the most plausible identification for **R1** (and RI of the previous work). With the added note that the HC2 coupling values are small, and therefore vulnerable to relatively small geometrical variations, we attribute the discrepancy between computation and experiment for line 7 and the HC2 coupling to the result of computation on an isolated vacuum-state molecule. The consequent difficulty in obtaining the actual geometry of the product in the solid state has been discussed previously.[14] Thus, it appears that the actual structure of **R1** differs from the optimized vacuum-state geometry of Hx^0_{-1} in such a way as to reduce the spin at N1 (or N3) and perhaps to increase the magnitude of spin at C2.[19]

Radical 2: The Electron-Gain Radical. As is shown in Figure 2, lines 1 and 3 exhibited similar EIE patterns, and both were observed to decay with no detectable successors on warming the crystals to ca. 50 K (shown in Figure 3). On the basis of the EIE, lines 1 and 3 were assigned to radical **R2**. Eigenvalues and eigenvectors for both are listed in Table 3. (Figure S2 of the Supporting Information shows the angular dependence of this coupling for three planes of data.)

Coupling 1 was assigned to an HC2 α-coupling since the eigenvectors for the minimum and intermediate values differ by 5.6 and 5.9° from the crystallographic C2−HC2 bond direction and the base perpendicular, respectively. The isotropic coupling indicates 0.30 spin density at C2 ($Q = -70$ MHz [15]), while the dipolar component indicates 0.28 ($Q^z_{dip} = 38.7$ MHz).[15,16] Coupling 3 was assigned to an HC8 α-coupling since $\hat{V}_{min}$ deviates 8.4° from the crystallographic C8−H bond and $\hat{V}_{mid}$ deviates 8.4° from the base perpendicular. The isotropic component of coupling 3 indicates 0.21 spin density at C8, while the dipolar component indicates 0.28 spin density.

The difference in spin densities indicated by the isotropic and dipolar components of coupling 3 indicates the likelihood of bending at the C8 position, probably that the C8−HC8 bond is bent out of the molecular plane. It is also notable that the HC2 and HC8 couplings have dipolar parts of similar magnitude indicating similar spin densities at the two positions.

With the goal of identifying the structure of **R2**, we calculated couplings expected from the electron-gain structures which seemed most plausible for the purine moiety: the product of electron gain by the native anionic base (Hx^{-2}_{-1}), the product of electron gain and protonation at N1 (Hx^{-1}), and the product of electron gain plus protonation at O6 ($Hx^{-1}_{-1,+6}$).[20] Calculations on all three structures predicted significant hyperfine couplings to HC2 and HC8 as were observed. (See entries 2−4 of Table 4.) However, for Hx^{-2}_{-1} and $Hx^{-1}_{-1,+6}$, the predicted HC8 couplings were significantly larger than experiment, and that for HC2 was significantly smaller. In contrast, for the Hx^{-1} structure, the situation was reversed.

Computational results from these negatively charged structures were quite sensitive to whether the basis sets included diffuse functions. For example, the N9−HN9 and C8−HC8 bonds were bent considerably in the gas-phase structure for Hx^{-2}_{-1} optimized without diffuse functions [B3LYP/6-31G-(d,p)]. In contrast, the corresponding structure optimized with diffuse functions [B3LYP/6-31+G(d,p)] was planar. Visualization of the HOMO for the latter structure showed it to exhibit severe diffuse character. This was reflected in the computed hydrogen hyperfine couplings which exhibited point-dipole character with small dipolar components rather than the normal α-coupling character exhibited by the experimental results.

Because of their sensitivity to diffuse functions, the computations indicate that the unpaired electron is loosely bound in a HOMO extending enough beyond the molecular framework that these radicals' surroundings can be significant in determining the experimentally observed results. In the crystal, a water molecule is positioned with hydrogen bonds to N1 and O6; O6 also accepts two additional hydrogen bonds, one from another water and the second from HO2′ of a neighboring molecule. Therefore, we undertook a set of computations to test the effect of nearby water on the hyperfine couplings from the gas-phase-optimized Hx^{-2}_{-1} structure.

Couplings for the $Hx^{-2}_{-1} + H_2O$ cluster geometry-optimized and calculated *without* diffuse functions (entry 5, Table 4) were virtually the same as those for $Hx^{-1}_{-1,+6}$ and Hx^{-2}_{-1} mentioned above. However, computations at the level of 6-311G(2d,p) on

TABLE 2: Computational Results for the Structures Hx_{-1}^{0} and $Hx_{-1,-9}^{-1}$ Compared with Experiment[a,b]

coupling atom	$Hx_{-1,-9}^{-1}$ iso.	$Hx_{-1,-9}^{-1}$ dip.	$Hx_{-1,-9}^{-1}$ eigenvectors ⟨a⟩	⟨b⟩	⟨c⟩	experiment iso.	experiment dip.	experiment eigenvectors ⟨a⟩	⟨b⟩	⟨c⟩	Hx_{-1}^{0} iso.	Hx_{-1}^{0} dip.	Hx_{-1}^{0} eigenvectors ⟨a⟩	⟨b⟩	⟨c⟩
		−3.77	0.4311	−0.8842	−0.1797		−2.84	0.482	−0.816	−0.318		−2.77	−0.8692	−0.4569	0.1889
HC2	−5.53	−2.00	−0.8669	−0.4612	0.1893	−3.56	−1.87	−0.846	−0.528	0.071	1.55	−1.18	0.2551	−0.7418	−0.6202
		5.77	0.2502	−0.0742	0.9653		4.71	0.226	−0.235	0.945		3.96	0.4235	−0.4909	0.7613
		−7.83	0.2939	−0.7784	−0.5547		−8.46	0.304	−0.767	−0.565		−9.17	0.3118	−0.8035	−0.5071
HC8	−12.45	−1.32	−0.8670	−0.4614	0.1882	−16.38	−1.31	−0.853	−0.483	0.198	−15.53	−0.83	−0.8693	−0.4567	0.1891
		9.15	0.4024	−0.4256	0.8105		9.76	0.424	−0.422	0.801		10.04	0.3835	−0.3819	0.8409
		−2.80					−0.78					−5.99			
N1	0.99	−2.77				3.42	−0.78				3.83	−6.07			
		5.58					1.56					12.06			
		−7.17					−8.88					−13.06			
N3	4.01	−6.99				12.94	−8.88				9.22	−12.85			
		14.17					17.76					25.91			
		−5.26													
N7	2.36	−4.97													
		10.23													

[a] Column headings "iso." and "dip." respectively indicate the isotropic and dipolar components of the hyperfine couplings. [b] All coupling values are MHz.

TABLE 3: Hyperfine Couplings for R2 Formed in Na^{+}·Inosine^{-}·2.5H_2O X-Irradiated at 10 K

coupling (line)	isotropic value[a,b]	principal value[b,c]	eigenvectors[a] ⟨a⟩	⟨b⟩	⟨c⟩
		−34.89(2)	−0.4421 (7)	0.8926 (5)	−0.0891 (15)
$R2_1$	−21.81(2)	−19.43(2)	−0.8733 (3)	−0.4056 (8)	0.2699 (9)
(line 1)		−11.10(2)	0.2048 (8)	0.1972 (16)	0.9588 (5)
		−28.17(2)	0.3404 (9)	−0.8230 (12)	−0.4547 (15)
$R2_2$	−14.39(4)	−11.60(2)	−0.8002 (5)	−0.5075 (12)	0.3195 (14)
(line 3)		−3.40(2)	0.4937 (7)	−0.2551 (15)	0.8314 (6)
		8.03	normal to the ring		
N7[c]	3.81	1.69	in the plane of the ring		
		1.69	in the plane of the ring		

directions from crystal structure	eigenvectors[a] ⟨a⟩	⟨b⟩	⟨c⟩
base perpendicular	−0.86845	−0.45239	0.20283
C8−H bond direction	0.36318	−0.30203	0.88141
C2−H bond direction	0.12216	0.15018	0.98108

[a] Numbers in parentheses are the estimated uncertainties in the respective values as reported by the statistical analysis. [b] Couplings in MHz. [c] See Spectrum Simulation for a description of the method used to evaluate these.

the cluster optimized at 6-31+G(d,p) gave HC2 and HC8 dipolar couplings more nearly equal, although still somewhat larger than the experimental values (entry 6, Table 4). Because of the additional water-like hydrogen bonding to O6, we then calculated the couplings for $Hx_{-1,+6}^{-1}$, Hx_{-1}^{-2}, and the Hx_{-1}^{-2} + H_2O cluster within a continuum dielectric ($\epsilon = 78.2$) using the PCM method of G03. For all cases, the respective dipolar couplings were very close to the experimental values (entries 7−9, Table 4). In fact, the b_+ values for Hx_{-1}^{-2} + H_2O are different from experiment by less than 10%.

The final step was to calculate couplings with the PCM procedure on variants of the structures in which the C8−HC8 bonds were artificially bent out of the molecular plane.[21] The structures optimized at 6-31+G(d,p) were nominally planar, but the experimental HC8 coupling showed evidence for pyramidal character of the bonds to C8. It is known that such character in the bonds to a center of spin affects the dipolar component minimally but causes the isotropic coupling component to become more positive.[22] The objective of this step was to test the possibility that computations with a reasonably bent structure could approximate the experimental values.

Calculated values from all three artificially bent structures provide reasonable approximations to the experimental isotropic and dipolar components (entries 10−12, Table 4). Thus, the couplings alone provide no conclusive basis for distinguishing among these as potential structures for **R2**. Likewise, the nitrogen couplings computed for the three structures are all consistent with the estimated experimental values. However, circumstantial evidence favors Hx_{-1}^{-2} for two reasons. First, Hx_{-1}^{-2} and Hx_{-1}^{-2} + H_2O are not really different for calculations where both are within the dielectric field of water. It is simply that the cluster explicitly includes a water molecule within the continuous water-like dielectric medium in which the PCM approach embeds the molecule. Second, transfer of a proton to O6 for forming $Hx_{-1,+6}^{-1}$ will certainly be inhibited by repulsive influences from the two waters also serving as hydrogen bond donors to O6. Thus, it seems less likely for O6 to attract a proton than for the water-like surroundings to enable the stability of the electron adduct.

On the basis of the reasoning above, we propose that the structure and conditions of entry 10 in Table 4 most accurately

TABLE 4: Computed Results for Various Structures and Conditions Compared to Experimental Results for R2[a,b]

entry no.	structure	OPT	SP	PCM	coupling	A_{iso}	b_-	b_0	b_+
1	experiment				HC2	−21.81	−13.08	2.38	10.71
					HC8	−14.39	−13.78	2.79	10.99
2	Hx^{-2}_{-1}				HC2	−12.12	−7.12	0.22	6.90
					HC8	47.88	−16.20	−3.63	19.83
3	Hx^{-1}				HC2	17.39	−24.01	−1.99	26.00
					HC8	−8.66	−4.99	−0.14	5.13
4	$Hx^{-1}_{-1,+6}$				HC2	−16.72	−9.19	−0.21	9.41
					HC8	35.09	−18.29	−1.20	19.49
5	$Hx^{-2}_{-1} + H_2O$				HC2	−15.25	−8.84	0.43	8.41
					HC8	45.23	−16.96	−3.35	20.31
6	$Hx^{-2}_{-1} + H_2O$	+			HC2	−25.49	−14.92	1.39	13.53
					HC8	−33.81	−19.85	4.15	15.69
7	Hx^{-2}_{-1}	+	+	X	HC2	−22.91	−12.76	1.03	11.73
					HC8	−28.01	−15.76	3.44	12.32
8	$Hx^{-1}_{-1,+6}$	+	+	X	HC2	−19.48	−9.92	−0.45	10.37
					HC8	−27.40	−14.74	2.05	12.69
9	$Hx^{-2}_{-1} + H_2O$	+	+	X	HC2	−23.27	−12.52	1.48	11.04
					HC8	−29.18	−15.90	4.01	11.89
10	Hx^{-2}_{-1}, 12° bend	+	+	X	HC2	−20.64	−11.50	0.78	10.72
					HC8	−15.82	−15.84	3.22	12.62
11	$Hx^{-1}_{-1,+6}$, 8° bend	+	+	X	HC2	−18.80	−9.59	−0.45	10.04
					HC8	−16.70	−14.47	1.21	13.26
12	Hx^{-2}_{-1}+ H_2O, 12° bend	+	+	X	HC2	−21.22	−11.42	1.21	10.21
					HC8	−17.28	−15.95	3.70	12.24

[a] "+" in the OPT column indicates geometries optimized at 6-31+G(d,p); others were optimized at 6-31G(d,p). "+" in the SP column indicates single-point calculations for EPR parameters using 6-311+G(2d,p); other single-point calculations used 6-311G(2d,p). "X" in the PCM column indicates a single point calculation using SCRF=PCM keyword. [b] All coupling values are in MHz.

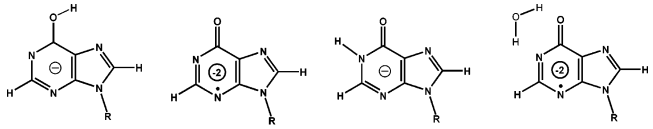

describes **R2** within the host crystal. Additional support for this conclusion is that the computation on the bent structure of entry 10 not only satisfactorily reproduces the experimental eigenvalues of the HC2 and HC8 couplings, it also reproduces the eigenvectors to good accuracy. For HC2, the angular differences between computed and experimental directions ($\hat{V}_{max}$, $\hat{V}_{mid}$, and $\hat{V}_{min}$, respectively) are 2.2, 4.1, and 4.1°; for HC8, the respective values are 1.5, 2.4, and 2.7°.

It should be noted that the PCM results are from single-point calculations using structures optimized in the gas phase. As such, they are not true equilibrium geometries for these cases. Nevertheless, the calculations support the identification that **R2** is the product of electron capture by the initially anionic parent purine moiety. Specifically, the calculations demonstrate that there exists a geometry and a combination of conditions for which such a radical ion can exhibit the observed set of hyperfine couplings. Moreover, the computations indicate that the observed couplings are strongly affected by the surroundings, namely the waters, a behavior reasonable for a doubly negative system where the added electron is expected to be loosely bound.

Radical 3: Unidentified Base-Centered Radical. On the basis of the EIE patterns shown in Figure 2, coupling 4 was assigned to radical **R3**. It was possible to collect ENDOR data in three independent planes for this coupling. (Figure S3 of the Supporting Information shows the angular dependence of this coupling for three planes.) Line 4 decayed in the range 200−250 K with no new lines appearing (not shown).

Coupling 4 was identified as an HC8 α-coupling since $\hat{V}_{min}$ and $\hat{V}_{mid}$ deviate 9.9° and 3.9° from the crystallographic C8−HC8 bond direction and the base perpendicular, respectively. The hyperfine coupling tensor derived from the data is listed in Table 5. From both the isotropic and dipolar coupling components, the spin at C8 is estimated to be 0.28 ($Q_{iso} = -70$ MHz [15] and $Q^z_{dip} = 38.7$ MHz[15,16]). These results also indicate that the bonds to C8 are coplanar in this product.

Although it is not possible to identify **R3** from coupling 4 alone, we note that a radical with a similar coupling was detected in the earlier study of anhydrous inosine crystals (labeled RVII in that study).[3] In that case, it was suggested that the radical was the result of deprotonation at N1 of the initial electron-loss product. However, based on the analysis of **R1** above, it is now evident that the product of N1-deprotonation was actually RI in the earlier work.

Radical R4: Ribose-Centered Radical. Only line 6 could be attributed to this radical by EIE as is shown in Figure 2. This low-amplitude line remained stable as crystals were warmed between10 and 100 K. On warming the crystal from 150 to 260 K, line 6 moved to a slightly lower frequency (not shown). (Figure S3 of the Supporting Information shows the angular dependence of this coupling for all three planes.) The

TABLE 5: Hyperfine Couplings for R3[a] Formed in Na^+·Inosine$^-$·2.5H_2O X-Irradiated at 10 K

coupling (line)	isotropic value[a,b]	principal value[b,c]	eigenvectors[a] ⟨a⟩	⟨b⟩	⟨c⟩
		−31.2 (2)	0.32526 (2)	−0.74675(1)	−0.58014 (1)
$R3_1$	−20.1(2)	−19.7 (2)	−0.86034 (1)	−0.48830 (2)	0.14619 (1)
(line 4)		−9.3 (2)	0.39245 (1)	−0.45157 (1)	0.80129 (1)
		18.6	normal to the ring		
N3[c]	6.22	0	in the plane of the ring		
		0	in the plane of the ring		
		21.6	normal to the ring		
N7[c]	7.20	0	in the plane of the ring		
		0	in the plane of the ring		

directions from crystal structure	eigenvectors[a] ⟨a⟩	⟨b⟩	⟨c⟩
base perpendicular	−0.86845	−0.45239	0.20283
C8−H bond direction	0.36318	−0.30203	0.88141
C2−H bond direction	0.12216	0.15018	0.98108

[c] Numbers in parentheses are the estimated uncertainties in the respective values as reported by the statistical analysis. [b] Couplings in MHz. [c] See Spectrum Simulation for a description of the method used to evaluate these. For these, the analysis gave small imaginary values for the in-plane components. For this reason, the values were simply set to 0.

TABLE 6: Hyperfine Couplings for R4[a] Formed in Na^+·Inosine$^-$·2.5H_2O X-Irradiated at 10 K

coupling (line)	isotropic value[a,b]	principal value[b,c]	eigenvectors[a] ⟨a⟩	⟨b⟩	⟨c⟩
		−94.06 (3)	0.6685(3)	−0.3286(4)	−0.6672(3)
$R4_1$	−59.22(3)	−56.53 (3)	0.5641(6)	0.8087(4)	0.1668(7)
(line 6)		−27.06 (3)	0.4847(2)	−0.4879(8)	0.7260(3)

directions from crystal structure	eigenvectors[a] ⟨a⟩	⟨b⟩	⟨c⟩
C5′-H(C5′a) bond direction	−0.23270	0.81832	0.52555
C5′-H(C5′b) bond direction	0.68274	0.67568	−0.27806
C2′-H(C2′) bond direction	−0.59281	0.31373	−0.74173
C3′-H(C3′) bond direction	−0.35204	−0.67703	−0.64630

[a] Structure **3a**. [b] Couplings in MHz.

corresponding hyperfine coupling tensor, typical for a •CH α-proton, was calculated from ENDOR data obtained at 10 K and is listed in Table 6. With $Q_{iso} = -70$ MHz,[15] the isotropic coupling indicates $\rho = 0.81$, and with $Q^z_{dip} = 38.7$ MHz,[15,16] the dipolar component indicates $\rho = 0.83$. These nearly-identical values indicate no detectable pyramidal character in the bonding to the CH_α π-fragment.

The eigenvectors associated with line 6 indicate that it is unlikely to be associated with the purine ring and thus likely to be from a ribose-centered radical. Such an α-proton coupling in the ribose could arise from a variety of events, such as dehydroxylation at C2′ or C3′, cleavage of the C4′-C5′ bond, net loss of either hydrogen from C5′ (Structure 3a), or cleavage of the N9−C1′ glycosidic bond (Structure 3b). In all cases, the resulting radical product is likely to undergo reorientation, perhaps to a very large degree, since the carbon at the center of spin will rehybridize to change the bonding geometry from tetrahedral to more nearly planar. Of the possibilities listed, radicals from net H loss at C5′ are well-known, while those from net dehydroxylation at C2′ or C3′ are unlikely since oxidation typically leads instead to dehydrogenation at C or O in sugars. In addition, the recent recognition that capture of low-energy electrons (LEEs) can lead to cleavage of the glycosidic bond[17] makes it important to consider the structure from rupture of the N9−C1′ bond (see the discussion associated with **R1** above). In particular, if the capture of an electron should lead to cleavage of the glycosidic bond, the greater electron affinity of the purine component vs the ribose makes the probability

TABLE 7: Computational Results for Structures 3a and 3b[a,b]

coupling	A_{iso}	b_{dip}	eigenvectors ⟨a⟩	⟨b⟩	⟨c⟩
		HC5′ Abstraction (Structure **3a**)			
		−35.07	0.7014	−0.4091	0.5837
HC52′	−38.68	−1.65	0.5882	0.7947	−0.1499
		36.73	−0.4025	0.4484	0.7981
		−6.65	−0.6482	0.3011	0.6994
HC4′	10.11	−4.04	0.5246	0.8424	0.1235
		10.69	0.5520	−0.4470	0.7039
		−12.65	−0.5959	0.6763	0.4331
HO5′	−7.46	−9.37	0.7250	0.6850	−0.0720
		22.02	0.3453	−0.2711	0.8985
		Glycosidic Cleavage (Structure **3b**)			
		−32.35	0.9179	0.3568	−0.1734
HC1′	−36.12	−2.11	−0.3792	0.6607	−0.6478
		34.46	−0.1166	0.6604	0.7418
		−6.02	0.7239	−0.6613	−0.1968
HC2′	65.31	−3.37	−0.0382	−0.3232	0.9456
		9.40	0.6889	0.6770	0.2592
		Experiment			
		−34.84	0.6685	−0.3286	0.6672
line 6	−59.22	3.69	0.5641	0.8087	−0.1668
		32.16	−0.4847	0.4879	0.7260

[a] Computed isotropic coupling values are in the column headed by A_{iso}, and dipolar values are in the column labeled b_{dip}. [b] All coupling values are given in MHz.

high that the electronic charge will reside on the purine fragment with the unpaired spin residing on the ribose. Thus, in an LEE event, the radical product of glycosidic bond cleavage is most likely to be a C1′-centered sugar radical.

Eigenvector $\hat{V}_{min}$ of **R2** deviates 26.7, 30.4, and 22.4° from the crystallographic C5′−HC51′ C5′−HC52′, and C1′−HC1′ bond directions, respectively. However, in view of the possibility for extensive reorientation, these correlations are of uncertain value. Therefore, we undertook a series of calculations on ribose structures derived from abstraction of either C5′ hydrogen (structure **3a**) or from cleavage of the N9−C1′ glycosidic bond (structure **3b**).

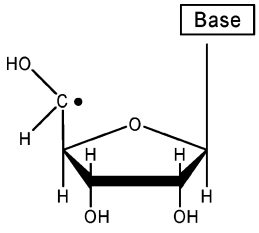

Structure 3a

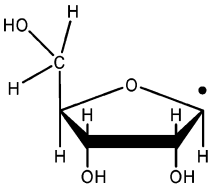

Structure 3b

In calculating the geometry from C5′ H-abstraction, the (crystal-based) coordinate set included the purine base but the positions of all purine atoms were frozen for the optimization. The objective was to anchor the ribose unit and prevent unrealistic reorientations. Although it was less clear how to achieve similar anchoring for the structure from glycosidic cleavage, we chose to freeze the coordinates of both C5′ and O5′. Results from the calculations are shown in Table 7. For HC5′ abstraction, the optimized structures were virtually identical regardless of the specific H5′ atom omitted from the initial coordinate set. As well, the results were the same for optimization [at 6-31G(d,p)] with or without diffuse functions. With the primary focus on properties of the calculated α-coupling (coupling values and dipolar directions) in comparison to the experimental results, it is clear that the result from abstraction of HC5′ provides a better match to the eigenvectors. (The computed isotropic components of the α-couplings for both structures are smaller than experiment and reflect a pyramidal geometry at the center of spin in both optimized geometries.) As well, this structure predicts a very small CCH_β coupling (to HC4′) while the C1′-centered structure from glycosidic bond cleavage predicts a β-coupling to HC2′ of approximately 65 MHz. In addition, the C5′-centered calculation predicts a highly anisotropic COH_β coupling. Although we identified no such coupling, the spectra contain unidentified ENDOR lines around 65 MHz. The corresponding radical centered on C5′ was also observed in the previous study of inosine where β-couplings to HO5′, C4′, and a δ-coupling to HO3′ were detected and analyzed.[3]

Radical 5: C8 H-Addition Radical. Figure 4 shows EPR and ENDOR spectra recorded after warming a crystal to room temperature. The EPR is dominated by a 3-line pattern characteristic of the well-known H-adduct species of which there can be two forms for inosine: addition at C2 or addition at C8. From EIE, shown in Figure 5, ENDOR lines 8−10 were assigned to **R5**, and Table 8 shows hyperfine tensors from these. (Figure S4, Supporting Information shows the angular dependence of these couplings for all three planes.) Coupling 8, from a nonexchangeable proton, is a typical C2−H α-coupling with eigenvectors for the minimum and intermediate principal values deviating only 0.7° and 0.3° from the C2−H bond direction

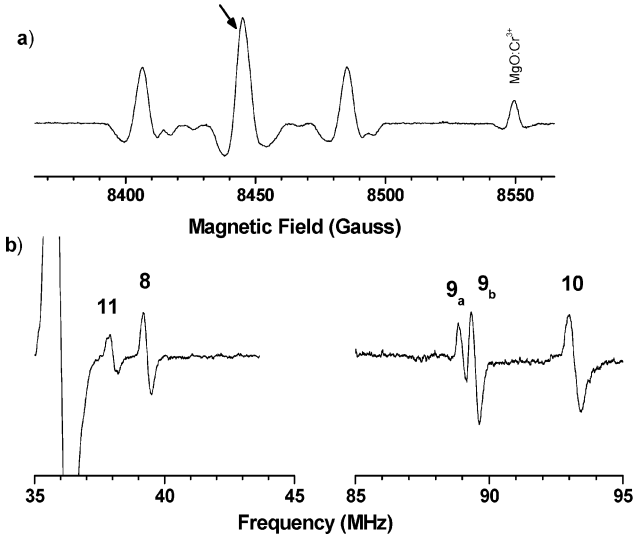

Figure 4. (a) EPR (second derivative) and (b) ENDOR from Na^+•Inosine$^-$•$2.5H_2O$ recorded at room temperature with the external field parallel to the ⟨*c*⟩ axis. At this position the magnetic field was approximately in the ring plane for one magnetic site. The arrow in the EPR spectrum indicates the magnetic field setting for the ENDOR scan.

and the base-perpendicular, respectively. With Q_{iso} of −70 MHz[15] the spin density at C2 is estimated as 0.19.

Coupling 8 unambiguously identifies **R5** as the C8 H-addition radical shown in structure **4**. (This radical was also present

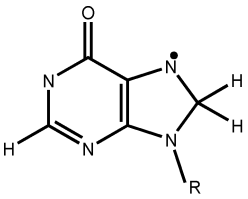

Structure 4: Hx^0_{+8}

immediately after irradiation at 6 K, as indicated by the presence of line 8 in Figure 1b. However, at 6 K the intensity of line 8 was much less than at room temperature.) Coupling tensors $\mathbf{R5}_2$ and $\mathbf{R5}_3$ are due to interactions with the two β-methylene protons at C8. The β-methylene couplings are nearly equal, indicating dihedral angles near 30°. The magnitudes of the hyperfine couplings are very similar to those of adenine C8 H-addition radicals (9-methyladenine[23] and deoxyadenosine monohydrate[24,25]).

It was not possible to obtain enough data to calculate a coupling tensor for line 11. This line must arise from a coupling to HC2, HC8, or a proton in the sugar since sodium inosine has no hydrogens at N1, N7, or N9. One possibility is that its source is the HC8 coupling from the C2 H-addition radical.

Spectrum Simulations. Gaussian calculations on radicals **R1** and **R2** discussed above predicted sufficient nitrogen spin density to affect the EPR patterns. Consequently, recreation of the EPR patterns, individually and in combination, with spectrum simulation techniques serves as confirmation of the radical structures proposed above. In addition, successful simulations will also provide an estimate of the relative populations of each radical form. Overall EPR patterns from the Na^+•Inosine$^-$•$2.5H_2O$ crystals were compact at most orientations, indicating limited contributions from nitrogen hyperfine couplings. Nevertheless, some orientations showed clear indication of nitrogen contributions.

TABLE 8: Hyperfine Couplings for R5[a] Formed in Na^+·Inosine$^-$·2.5H_2O X-Irradiated at Room Temperature

			eigenvectors[a]		
coupling (line)	isotropic value[a,b]	principal value[b,c]	⟨*a*⟩	⟨*b*⟩	⟨*c*⟩
		−20.88(2)	−0.473(2)	0.877(1)	−0.087(2)
$R5_1$	−13.51(2)	−13.41(2)	0.874(1)	0.454(2)	−0.172(2)
(line 8)		−6.24(2)	0.112(2)	0.158(3)	0.981(0)
		112.70(2)	0.816(1)	−0.311(5)	0.488(1)
$R5_2$	107.26(2)	105.29(2)	0.051(2)	−0.802(5)	−0.595(8)
(line 9)		103.79(2)	0.576(1)	0.511(6)	−0.638(6)
		118.70(2)	0.068(2)	−0.748(12)	0.660(7)
$R5_3$	113.32(2)	111.27(2)	0.493(0)	0.600(4)	0.629(8)
(line 10)		109.94(2)	0.867(0)	−0.283(6)	−0.410(9)

	eigenvectors[a]		
directions from crystal structure	⟨*a*⟩	⟨*b*⟩	⟨*c*⟩
base perpendicular	−0.86845	−0.45239	0.20283
C8−H bond direction	0.36318	−0.30203	0.88141
C2−H bond direction	0.12216	0.15018	0.98108

[a] Structure **4**. [b] Numbers in parentheses are the estimated uncertainties in the respective values as reported by the statistical analysis. [c] Couplings in MHz.

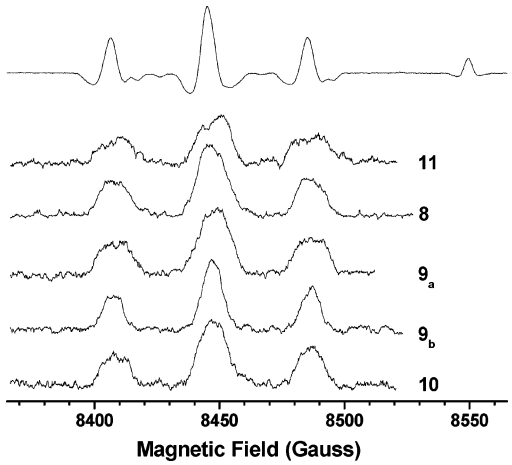

Figure 5. EPR (top) and EIE responses (lower 5) from each ENDOR line shown in Figure 4b. The EIE patterns are similar for all ENDOR lines except line 11. Lines 9a and 9b are the same coupling but from radicals in the two distinct magnetic sites. Since line 9 is more anisotropic than the other two, slight misorientation leads to doubling of the lines as seen in Figure 4b. (The EPR line near 8550 G is from the MgO:$Cr3^+$ reference sample.).

Our approach to the simulations was as described previously.[5] The nitrogen couplings listed in the tables above were obtained with those methods by simulating the EPR at three magnetic field positions: field along ⟨*a*⟩, ⟨*b*⟩, and in the ring plane for rotation about ⟨*a*⟩. Figure 6 shows simulated and the experimental spectra for three different magnetic field orientations. The simulations indicated relative radical concentrations as follows: **R1** = 55.7%, **R2** = 23.6%, **R3** = 15.0%, and **R4** = 5.7%. Because the relatively low-resolution character of the spectra makes the uncertainty in these results high, they should be considered only as estimates.

Discussion: Proton-Transfer Behavior

A central focus of this series of studies is identification and description of the proton-transfer behavior of the primary ionized molecular species. Proton transfers are an important stage in the evolution of radiation-induced damage. They are slower than electron transfers, but the stability of primary ionic species can be determined by whether intermolecular proton transfers occur before electron−hole recombination.[2] If recombination occurs first, there will be no lasting effects of the ionization; however if proton transfers occur before recombination, the ionization produces neutral radicals which can—and will—react further to produce the ultimate chemical consequences of ionization.

Because of their far greater mass, protons are much less mobile than electrons. Thus, at the experimental temperatures for this study (10 K), the most probable proton transfers are those between neighbors, and hydrogen bonds are most probable routes. Structure **5** indicates the arrangement of hydrogen bonds

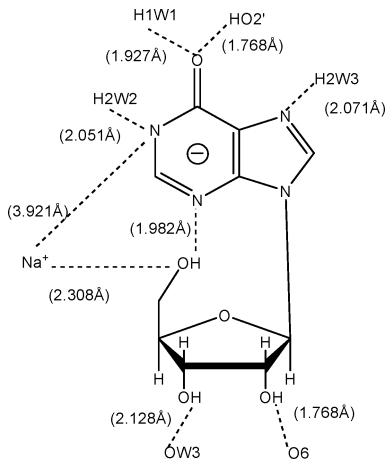

Structure 5. Hydrogen bonding arrangements

and close contacts in the Na^+·Inosine$^-$·2.5H_2O crystals. (In the crystal, all available hydrogen bond acceptors and donors participate in hydrogen bonds or close associations.) Particularly notable points are as follows: (1) the Na^+ ion, strongly associated with the waters in the vicinity of sugar O5′, is 3.9 Å from N1 and is more that 4.0 Å from other base atoms; (2) N1, the deprotonated site, is hydrogen-bonded/closely associated with a water proton at the distance of 2.051 Å; (3) the shortest hydrogen bond is between O6 and HO2′ of a neighboring molecule (1.768 Å); (4) O6 accepts a second hydrogen bond from a water proton (the "0.5" water) with the length 1.927 Å and is closely associated with a hydrogen from still another water (d = 2.579 Å); (5) N3 accepts an intramolecular hydrogen bond from HO5′ (1.982 Å).

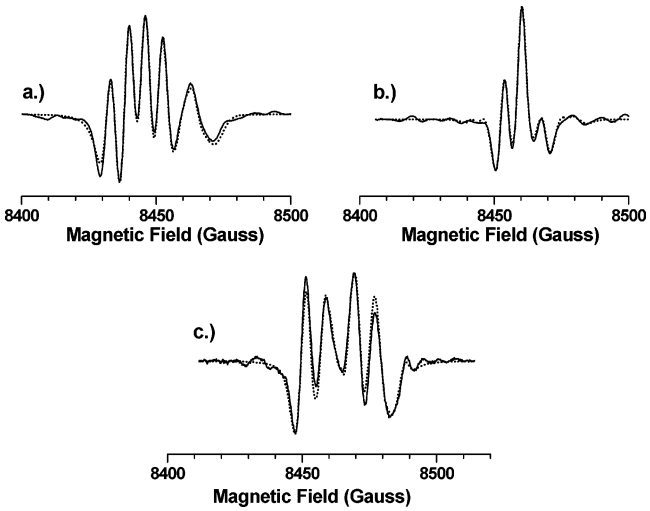

Figure 6. Comparison of simulated (dotted lines) and experimental (solid lines) EPR spectra (second derivative) from $Na^+ \cdot Inosine^- \cdot 2.5H_2O$ for three different positions of the magnetic field in the ab crystallographic plane: (a) with the magnetic field parallel to the $\langle b \rangle$ axis, (b) with the magnetic field in the ring plane for one of the magnetic sites, and (c) with the magnetic field parallel to the $\langle a \rangle$ axis.

In the discussion above, the conclusions were that radicals **R1** and **R2** are the primary electron-loss and electron-gain products of the hypoxanthine base. It is unusual for the primary products to be stabilized in crystals without intermolecular proton transfers. Qualitative summaries of several studies in fact concluded that product stabilization depended on hydrogen bonding networks allowing concerted proton transfers which move the net charge two or more molecules away.[24,25] In the $Na^+ \cdot Inosine^- \cdot 2.5H_2O$ system, the absence of a proton at N1 in the parent structure renders the purine base without protons capable of serving as hydrogen bond donors. However, previous work led to the suggestion that cytosine and adenine nucleotides would deprotonate at C1′ under conditions inhibiting to deprotonation from the base.[25,26] It is therefore notable in this case that **R1** was detected as the product of one-electron oxidation and no evidence was detected for the product of HC1′ abstraction. Likewise, the evidence for **R2** indicates shallow trapping of the electron. The indicated environmental effects on the hyperfine couplings suggests trapping somewhat like that reported previously for electrons in sugars.[27] In this case, rather than being trapped interstitially, the electron is trapped by the molecule itself. However, the molecule is within surroundings somewhat like that created by the polyhydroxy environment establishing the electron traps in sugars. Thus, rather than being localized, the electron is "lightly attached" to the molecular framework and the unpaired spin is delocalized around the hypoxanthine unit. With this arrangement, the local electric fields generated by the anionic character of the surrounding molecules evidently establishes a marginally stable trapping site for additional negative charge in the $Na^+ \cdot Inosine^- \cdot 2.5H_2O$ system.

Summary and Conclusions

In summary, upon X irradiation at 10 K, the $Na^+ \cdot Inosine^- \cdot 2.5H_2O$ system stabilized five radical products, four of which could be identified from the EPR/ENDOR data. **R1** was the product of electron loss from the initially anionic N1-deprotonated hypoxanthine unit. As such, this product is equivalent to the N1-deprotonated electron-loss product of hypoxanthine. On the basis of the similarity of hyperfine couplings, **R1** is apparently the same as an unidentified product previously reported from X irradiated inosine;[3] therefore, these results allow that product to be identified. **R2** was the product of electron gain by the initially anionic hypoxanthine unit. Unusual about **R1** and **R2** in this crystal system is that they were primary electron-loss and electron-gain products stabilized without intermolecular proton transfers. Warming the crystals to ca. 50 K led to simultaneous disappearance of both, probably by electron−hole recombination. **R3** could not be identified. On the basis of its single hyperfine coupling and computational modeling, **R4** was identified as the product of net dehydrogenation from C5′ of the ribose unit. **R5**, detected at low temperature but studied at room temperature, was identified as the product of net hydrogen addition to C8.

Of these, the most unusual was **R2.** Its identification as the primary electron-gain product of the initially anionic purine parent was established primarily on the basis of a computational model including the host environment. The model yielding results most compatible with experiment indicated that the unpaired electron of the doubly negative product was weakly bound making the observable hyperfine parameters strongly affected by the dielectric properties of the surroundings. As well, the experimental results indicated nonplanarity of the bonds to HC8, a property supported by the computations on structures with artificially adjusted geometries. However, the structural model providing computational couplings (coupling values and characteristic directions) most compatible with experiment was not that of full geometry optimization under the set of conditions indicated by the analysis. This indicates that further development of computational methodology is necessary for successful ab initio description of molecular systems such as **R2** within their host environment.

Acknowledgment. The early stages of this work were supported by NIH Grant CA36810. The authors also wish to thank Dr. Tomasz Wasowicz for technical assistance in obtaining and analyzing the spectra.

Supporting Information Available: Figures showing the angular dependence of the coupling tensors for **R1** from $Na^+ \cdot Inosine^-$ (Figure S1), for **R2** from $Na^+ \cdot Inosine^-$ (Figure S2), for **R3** and **R4** from $Na^+ \cdot Inosine^-$ (Figure S3), and for **R5** from $Na^+ \cdot Inosine^-$ at room temperature (Figure S4). This material is available free of charge via the Internet at http://pubs.acs.org.

References and Notes

(1) Steenken, S. *Chem. Rev.* **1989**, *89*, 503.
(2) Steenken, S. *Free Radical Res. Commun.* **1992**, *16*, 349.
(3) Hole, E. O.; Nelson, W. H.; Sagstuen, E.; Close, D. M. *Radiat. Res.* **1992**, *130*, 148.
(4) Tokdemir, S.; Nelson, W. H. *Radiat. Res.* **2005**, *163*, 663.
(5) Tokdemir, S.; Nelson, W. H. *J. Phys. Chem. A* **2005**, *109*, 8732.
(6) Klüfers, P.; Mayer, P. *Acta Crystallogr.* **1996**, *C52*, 2970.
(7) Schonland, D. S. *Proc. Phys. Soc* **1959**, *73*, 788.
(8) (a) Nelson, W. H.; Hole, E. O.; Sagstuen, E.; Close, D. M. *Int. J. Radiat. Biol.* **1988**, *54*, 963. (b) Kang, J.; Tokdemir, S.; Shao, J.; Nelson, W. H. *J. Magn. Reson.* **2003**, *165*, 128.
(9) Frisch, M. J.; Trucks, G. W.; Schlegel, H. B.; Scuseria, G. E.; Robb, M. A.; Cheeseman, J. R.; Montgomery, J. A., Jr.; Vreven, T.; Kudin, K. N.; Burant, J. C.; Millam, J. M.; Iyengar, S. S.; Tomasi, J.; Barone, V.; Mennucci, B.; Cossi, M.; Scalmani, G.; Rega, N.; Petersson, G. A.; Nakatsuji, H.; Hada, M.; Ehara, M.; Toyota, K.; Fukuda, R.; Hasegawa, J.; Ishida, M.; Nakajima, T.; Honda, Y.; Kitao, O.; Nakai, H.; Klene, M.; Li, X.; Knox, J. E.; Hratchian, H. P.; Cross, J. B.; Adamo, C.; Jaramillo, J.; Gomperts, R.; Stratmann, R. E.; Yazyev, O.; Austin, A. J.; Cammi, R.; Pomelli, C.; Ochterski, J. W.; Ayala, P. Y.; Morokuma, K.; Voth, G. A.; Salvador, P.; Dannenberg, J. J.; Zakrzewski, V. G.; Dapprich, S.; Daniels, A. D.; Strain, M. C.; Farkas, O.; Malick, D. K.; Rabuck, A. D.; Raghavachari, K.; Foresman, J. B.; Ortiz, J. V.; Cui, Q.; Baboul, A. G.; Clifford, S.; Cioslowski, J.; Stefanov, B. B.; Liu, G.; Liashenko, A.; Piskorz,

P.; Komaromi, I.; Martin, R. L.; Fox, D. J.; Keith, T.; Al-Laham, M. A.; Peng, C. Y.; Nanayakkara, A.; Challacombe, M.; Gill, P. M. W.; Johnson, B.; Chen, W.; Wong, M. W.; Gonzalez, C.; Pople, J. A. Gaussian 03. Rev. B.04 ed.; Gaussian Inc.: Pittsburgh, PA, 2003.

(10) (a) Becke, A. D. *J. Chem. Phys.* **1993**, *98*, 1372. (b) Stephens, P. J.; Devlin, F. J.; Chabalowski, C. F.; Frisch, M. J. *J. Phys. Chem.* **1994**, *98*, 11623. (c) Lee, C.; Yang, W.; Parr, R. G. *Phys. Rev. B* **1988**, *37*, 785.

(11) (a) Ditchfield, R.; Hehre, W. J.; Pople, J. A. *J. Chem. Phys.* **1971**, *54*, 724. (b) Hehre, W. J.; Ditchfield, R.; Pople, J. A. *J. Chem. Phys.* **1972**, *56*, 2257. (c) Hariharan, P. C.; Pople, J. A. *Mol. Phys.* **1974**, *27*, 209. (d) Gordon, M. S. *Chem. Phys. Lett.* **1980**, *76*, 163. (e) Hariharan, P. C.; Pople, J. A. *Theor. Chim. Acta* **1973**, *28*, 213. (f) McLean, A. D.; Chandler, G. S. *J. Chem. Phys.* **1980**, *72*, 5639. (g) Krishnan, R.; Binkley, J. S.; Seeger, R.; Pople, J. A. *J. Chem. Phys.* **1980**, *72*, 650. (h) Clark, T.; Chandrasekhar, J.; Spitznagel, G. W.; Schleyer, P. v. R. *J. Comput. Chem.* **1983**, *4*, 294. (i) Frisch, M. J.; Pople, J. A.; Binkley, J. S. *J. Chem. Phys.* **1984**, *80*, 3265.

(12) Ban, F.; Gauld, J. W.; Wetmore, S. D.; Boyd, R. J. The calculation of the hyperfine coupling tensors of biological radicals. In *Progress in Theoretical Chemistry and Physics*; Lund, A., Shiotani, M., Eds.; Kluwer: Dordrecht, The Netherlands, 2003; Vol. 10; pp 239−265.

(13) Pauwels, E.; Van Speybroeck, V.; Vanhaelewyn, G.; Callens, F.; Waroquier, M. *Int. J. Quantum Chem.* **2004**, *99*, 102.

(14) Vanhaelewyn, G. C. A. M.; Jansen, B.; Pauwels, E.; Sagstuen, E.; Waroquier, M.; Callens, F. J. *J. Phys. Chem. A* **2004**, *108*, 3308.

(15) Bernhard, W. A. *J. Chem. Phys.* **1984**, *81*, 5928.

(16) Gordy, W. *Theory and Applications of Electron Spin Resonance*; Wiley: New York, 1980.

(17) The superscripts of the structure symbols indicate the net charge, and the subscripts indicate the loss (−) or gain (+) of a proton. For example $Hx^{-1}_{-1,-9}$ is the standard hypoxanthine structure with net charge −1, without the proton normally at N1, and without the proton normally at N9.

(18) (a) Abdoul-Carime, H.; Sanche, L. *Radiat. Res.* **2001**, *156*, 151. Li, X.; (b) Sevilla, M. D.; Sanche, L. *J. Am. Chem. Soc.* **2003**, *125*, 13668. (c) Zheng, Y.; Cloutier, P.; Hunting, D. J.; Wagner, J. R.; Sanche, L. *J. Am. Chem. Soc.* **2004**, *126*, 1002.

(19) We note that single-point calculation of the EPR parameters with the same structure but using 6-311+G(2d,p) within a continuum dielectric field (PCM) led to computed eigenvectors for HC2 more nearly consistent with experiment.

(20) The dipolar portion of the coupling is more reliable than the isotropic component as an indicator of spin distribution. Thus, the comparisons mentioned in the text are between the most positive dipolar components of the respective couplings.

(21) The bending was accomplished by rotating the C8−HC8 bond about a direction perpendicular to C8−HC8 and coplanar with N7−C8−N9.

(22) Erling, P. A.; Nelson, W. H. *J. Phys. Chem. A* **2004**, *108*, 7591.

(23) Close, D. M.; Nelson, W. H.; Sagstuen, E.; Hole, E. O. *Radiat. Res.* **1994**, *137*, 300.

(24) (a) Bernhard, W. A.; Barnes, J.; Mercer, K. R.; Mroczka, N. *Radiat. Res.* **1994**, *140*, 199. (b) Bernhard, W. A.; Mroczka, N.; Barnes, J. *Int. J. Radiat. Biol.* **1994**, *66*, 491.

(25) Nelson, W. H.; Sagstuen, E.; Hole, E. O.; Close, D. M. *Radiat. Res.* **1998**, *149*, 75.

(26) Malone, M. E.; Cullis, P. M.; Symons, M. C. R.; Parker, A. W. *J. Phys. Chem.* **1995**, *99*, 9299.

(27) Box, H. C.; Budzinski, E. E.; Freund, H. G. *J. Chem. Phys.* **1978**, *69*, 1309.